Journal of Power Sources 253 (2014) 114–122

Contents lists available at ScienceDirect

Journal of Power Sources

journal homepage: www.elsevier.com/locate/jpowsour

High performance Bi-layered electrolytes via atomic layer deposition for solid oxide fuel cells

Youngseok Jee [a], Gu Young Cho [b], Jihwan An [c], Hae-Ryoung Kim [d], Ji-Won Son [d], Jong-Ho Lee [d], Fritz B. Prinz [c], Min Hwan Lee [a,*], Suk Won Cha [b]

[a] School of Engineering, University of California, Merced, 5200 N. Lake Rd., Merced, CA 95343, USA
[b] School of Mechanical and Aerospace Engineering, Seoul National University, Seoul 151-744, Republic of Korea
[c] Department of Mechanical Engineering, Stanford University, Stanford, CA 94305, USA
[d] High Temperature Energy Materials Center, Korea Institute of Science and Technology, Seoul 136-791, Republic of Korea

HIGHLIGHTS

- Feasibility of ultra-thin protective layer for a stable and high-performing SOFC.
- Validates a theoretical guideline for bi-layered electrolytes prepared by ALD.
- Chemical and structural stability of bi-layered electrolytes in various environments.
- Useful design/operational guidelines for IT-SOFCs using bi-layered electrolyte scheme.

GRAPHICAL ABSTRACT

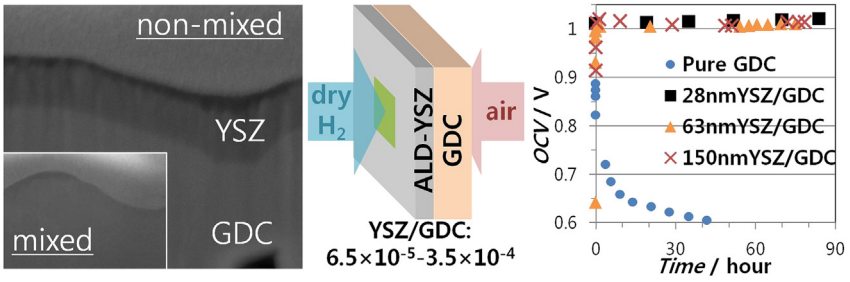

ARTICLE INFO

Article history:
Received 29 August 2013
Received in revised form
20 November 2013
Accepted 1 December 2013
Available online 12 December 2013

Keywords:
solid oxide fuel cell
Atomic layer deposition
YSZ/GDC bi-layer
Sintering temperature
Ceria reduction

ABSTRACT

This study investigates the functionality of bi-layered electrolytes in intermediate temperature solid oxide fuel cells. A thin yttria-stabilized zirconia (YSZ) layer is expected to protect the underlying gadolinia doped ceria (GDC) electrolyte from being chemically reduced and significantly improve cell stability and durability. Although a thinner YSZ layer is preferable to minimize ohmic loss, there are limitations as to how thin the YSZ film can be and still serves as a valid protection layer. The limitation is partially attributed to the inter-diffusion and significant morphological changes during the high temperature sintering processes. In this study, a stable operation was demonstrated for extended duration (>80 h) with only a 28 nm YSZ layer (corresponding to a YSZ/GDC thickness ratio of 6.5×10^{-5}) when limitations in both fabrication (<~800 °C) and operating conditions (<~600 °C, dry H_2) were imposed. Furthermore, the functionality of a protection layer with a given thickness was found to strongly depend on the method of depositing the protective layer. Protective layers deposited by atomic layer deposition (ALD) can be much thinner than those prepared by physical vapor deposition; the YSZ/GDC thickness ratio for a stable operation approached close to a theoretical value when the ALD was used.

1. Introduction

Intermediate temperature (600–800 °C) solid oxide fuel cells (IT-SOFCs) have been actively studied due to many advantages over conventional SOFCs in terms of availability of sealants and metal interconnectors, cost effectiveness, degradation rate, packaging

* Corresponding author. Tel.: +1 209 228 4186; fax: +1 209 228 4047.
E-mail address: mlee49@ucmerced.edu (M.H. Lee).

0378-7753/$ – see front matter © 2013 Elsevier B.V. All rights reserved.
http://dx.doi.org/10.1016/j.jpowsour.2013.12.001

volume, start-up time and device applicability [1]. However, a decrease in operating temperature causes a significant sacrifice of ionic conductivity, which motivated researchers to seek electrolytes with much higher conductivity than yttria-stabilized zirconia (YSZ). Doped ceria such as gadolinia doped ceria (GDC) can be a good electrolyte candidate for IT-SOFCs because they are ~5 times more conductive than YSZ at 600 °C [2–4]. However, doped ceria is vulnerable to chemical instability in a low oxygen partial pressure environment. Ceria reduction gives rise to electronic conductivity, and thus lowers the open circuit voltage (OCV) and power density of the cell [5]. It can also cause internal stress owing to the resulting volumetric expansion, which will negatively affect the gas tightness and the structural reliability of cells [6,7].

Significant efforts to improve chemical stability while maintaining high ionic conductivity have resulted in various types of bi-layered electrolyte configurations [8–12]. The YSZ/GDC bi-layered electrolyte has been arguably one of the most popular approaches among the bi-layer schemes [13–18]. A thin YSZ film of the YSZ/GDC system serves as a protective layer against chemical degradation of ceria in a reducing gas environment.

An important issue of zirconia/ceria based bi-layered structure is inter-diffusion between the two layers. Tsoga et al. reported that YSZ and GDC layers were mixed and a resulting secondary phase ($Ce_{0.37}Zr_{0.38}Gd_{0.18}Y_{0.07}O_{1.87}$) has a lower ionic conductivity than YSZ by two orders of magnitude at 800 °C [19]. In another study, Zhou et al. showed that the diffusion of Ce into YSZ causes an increase in electronic conductivity and a decrease in ionic conductivity [20]. This is a critical issue for a nano-thin YSZ-based bi-layered electrolyte since a slight intermixing can disrupt the functionality of YSZ as a protection layer. Another issue was micro-cracks generated in the GDC layer during volumetric expansion under reducing conditions. This needs to be minimized because even a small morphological change on the surface of GDC can affect the adhesion and gas tightness of the neighboring YSZ layer. The volume expansion is caused by the replacement of Ce^{4+} ions (with an ionic radius of 0.97 nm) with larger Ce^{3+} ions (with an ionic radius of 1.14 nm) during the reduction process [21]. With these issues in mind, we examined the compositional and morphological changes of the bi-layered electrolytes with multi-thickness YSZ layers on GDC substrates under various temperatures and gas environments.

There are several requirements to obtain a high-performance protective layer. We need to be able to fine-control the optimal YSZ thickness to avoid redundant ohmic loss. A pinhole-free and dense layer is also needed to prevent the direct access of fuel gas to the underlying ceria layer. High film uniformity would suppress the formation of "hot spots" where electrical current is concentrated and/or ceria reduction is facilitated due to a thinner protection layer. In order to meet all these requirements, we employed atomic layer deposition (ALD) technique, which is known to provide pinhole free and dense layers with high uniformity, superior step coverage and accurate thickness control capabilities [22]. In this report, we also compare the functionality of YSZ protective layer prepared by the ALD with those by physical vapor deposition (PVD) techniques.

2. Experimental

We operated and characterized mixed-electrolyte cells exposed to a high temperature fabrication condition. Then we performed compositional and morphological stability tests in various environments for bi-layered samples without electrodes fabricated via ALD. Obeying the restrictions for operation and fabrication processes, we tested non-mixed bi-layered electrolyte cells and compared these results to the reported data from other deposition methods.

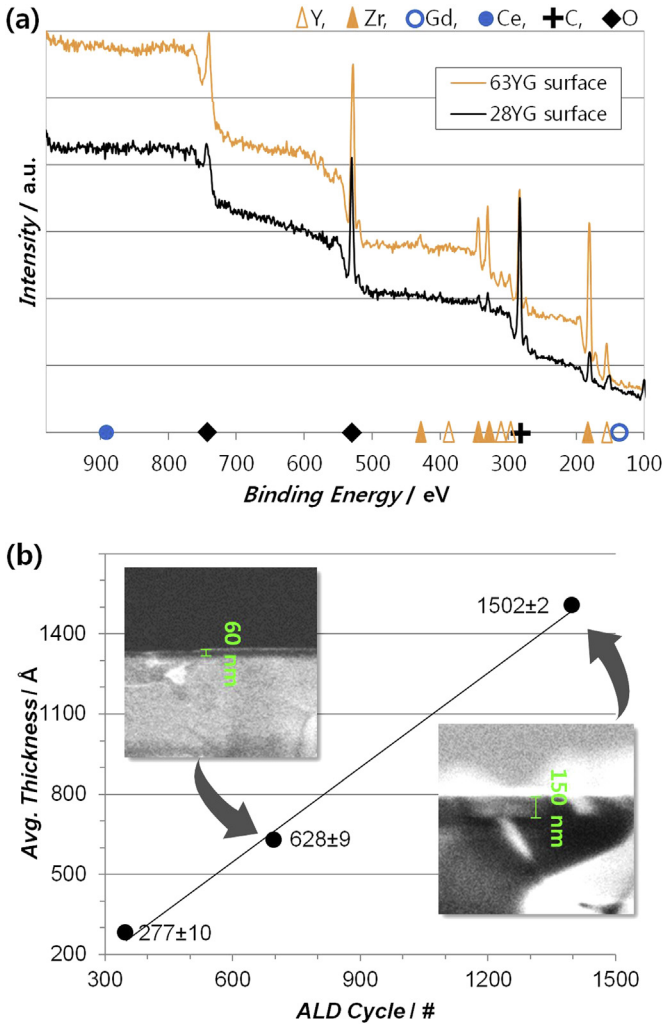

Fig. 1. Characterization results from as-deposited YSZ/GDC electrolytes. (a) XPS profiles for the 28YG and 63YG samples; no Gd or Ce peak found on their surfaces, and (b) ellipsometry thickness with the ALD pulsing cycles of 350, 700 and 1400 (corresponding to 28YG, 63YG and 150YG, respectively) and cross-sectional SEM images of 63YG and 150YG.

2.1. Bi-layered cell preparation

In order to fabricate GDC samples, 10% GDC powder ($(Ce_{0.9}Gd_{0.1})O_{1.95}$, GDC10-HP; NexTech Materials Ltd., USA) was pressed at 2000 bar in a cold isostatic press (CIP) followed by a sintering process at 1450 °C. The resulting GDC was grounded to a thickness of ~500 μm and the sliced pieces were thinned down to 430 μm with a mechanical polisher. Then, a firing process was performed at 600 °C for 2 h to eliminate polishing agents. The resulting average roughness was 134 nm. We applied the ALD technique to deposit a YSZ layer on the GDC. Tetrakis(dimethylamido)zirconium ($[(CH_3)_2N]_4Zr$, Sigma–Aldrich®, USA) and tris(methylcyclopentadienyl)yttrium ($((CH_3C_5H_4)_3Y$, Strem Chemicals, Inc., USA) were used as the precursors of the zirconia and yttria, where the ratio of pulsing numbers between zirconia and yttria was 7:1 [23]. The reaction chamber was controlled at 230 °C, while distilled water was used as the oxidant. The cycle numbers for the YSZ deposition were fourfold: 0, 350, 700 and 1400 cycles. The mole fraction of yttria in the YSZ is found to be ~7% from the X-ray photoelectron spectroscopy (XPS) analysis shown in Fig. 1(a).

For the cells exposed to high sintering temperatures, GDC–NiO cermet (50:50) and GDC–lanthanum strontium cobalt ferrite

(GDC–LSCF, 50:50) were used for the anodes and cathodes, respectively. Both electrodes were screen-printed followed by a 2 h-long sintering process. We maintained a sintering temperature of 1400 °C for anodes and 1200 °C for cathodes. The rate of heating and cooling for the sintering was 3 °C min^{-1}, which was found to be slow enough not to cause any significant cracking or fracturing in the final cells. The thickness of each electrode was 30 μm.

For the cells not exposed to high temperature, Pt sputter depositions (AT12, Atech Co., Korea) on both sides of the ALD-YSZ bi-layered electrolyte completed the cell fabrication process. Sputter deposition was performed at the Ar pressure of 8 Pa and ambient temperature to obtain a porous layer. 200 W DC power was used and the target-to-sample distance was 10 cm.

With the purpose of minimizing the surface morphology-originated artifacts for atomic force microscopy (AFM) and maximizing the accuracy of depth profiling for XPS in stability tests, GDC surfaces were polished using a chemical mechanical polisher (CMP, Brand Laser Optics & MFG, USA) before depositing YSZ layers. After the firing process at 600 °C and the ALD-YSZ layer deposition on the polished GDC, the final roughnesses of all the four kinds of samples with different YSZ thicknesses were below 2 nm. Then we exposed the samples to air with ambient temperature, 600, 800, 1200 and 1500 °C for 5 h, and to humidified H_2 ($H_2O/(H_2 + H_2O) = 3\%$) with 600 and 800 °C.

2.2. Material characterizations

Field emission scanning electron microscope (FE-SEM) systems with high magnification and focused ion beam (FIB) systems (Strata 235DB dual-beam, FEI, USA, Quanta 3D FEG, FEI, USA and Supra 55VP, Carl Zeiss, Germany) were used to observe the top view and the cross-sectional bi-layers of YSZ/GDC. The thickness of ALD-YSZ on the fine-polished GDC surface was quantified using a single-wavelength ellipsometer (L116C, Gaertner Scientific Corp. USA). The ellipsometer was set to an incident angle of 70° and a refractive index of 2.13 for the YSZ film. XPS (VersaProbe Scanning XPS Microprobe, PHI, USA and AXIS-HSi, Kratos Analytical, USA) was used to analyze the chemical profile of bi-layered electrolytes along the depth direction. An AFM (Nano Station II, Surface Imaging Systems, Germany) was used to characterize the surface morphology and roughness. All the images were obtained using the contact mode with the scan size of 4 × 4 μm^2.

2.3. Electrochemical characterizations

The custom-built fuel cell test station was mainly composed of an electric tube furnace with a temperature controller, cell supporting jigs, a pressing unit, gas flow tubes with mass flow controllers, and a humidifier at the anode line. Measurements of OCVs were conducted using an electrochemical potentiostat (SI 1287, Solartron Analytical, UK, and SP-240, Bio-logic, France). Ni and Pt meshes were used as current collectors on anode and cathode sides, respectively. The pressing unit applied 0.5 kgf between the upper and lower supporting jigs during measurements to ensure gas tightness. A gold O-ring (GG030020, Scientific Instrument Services Inc., USA) was used as a gas sealant.

In the OCV measurements for the cells exposed to high sintering temperatures, humidified 5% H_2 ($H_2O/(H_2+N_2+H_2O) = 3\%$; $H_2/(H_2+N_2) = 5\%$) and air were supplied to the anode and cathode, respectively. The gas pressure throughout the experiment was 2 atm and the cell temperature during the measurement was 600 °C. For the experiments of the cells not exposed to high temperature, 99.999% dry H_2 and air (both at 2 atm) were used as a fuel and an oxidant gas.

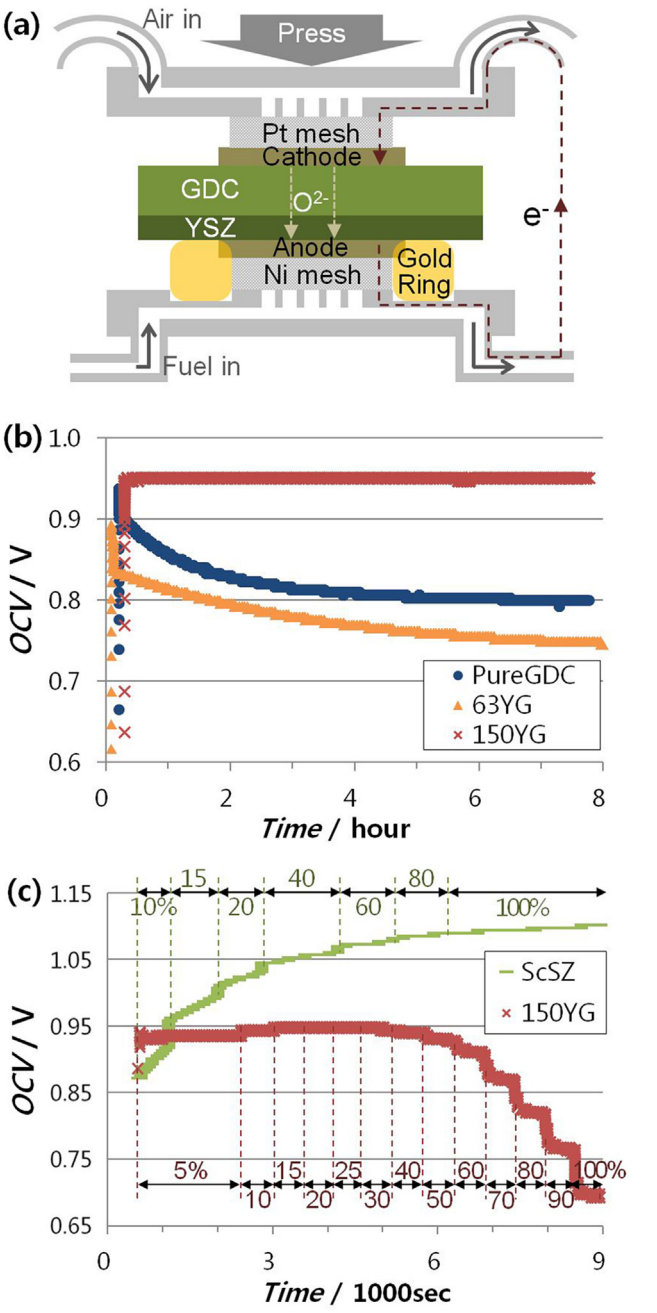

Fig. 2. (a) A simplified drawing of the electrochemical measurement setup. (b) OCV results measured at 600 °C for the pure GDC (blue circle), 63YG (yellow triangle) and 150YG (red cross) cells that have been exposed to a sintering temperature of 1400 °C. Only the 150YG cell showed the protection functionality in humidified 5% H_2 fuel environment. (c) Time evolution of OCV measured through an ScSZ-based cell (green) and a 150YG-based cell (red); the ScSZ cell showed an OCV very close to the thermodynamically predicted values while the 150YG cell suffered from larger contributions of ceria reduction under H_2 concentrations of $>\sim$20% (For interpretation of the references to color in this figure legend, the reader is referred to the web version of this article.).

3. Results and discussion

3.1. Cells exposed to high temperature fabrication processes

As mentioned earlier, a thinner YSZ layer is advantageous to minimize additional ohmic loss. However, there are limitations on how thin a YSZ layer can be because a nano-thin protection layer

may not survive the usual sintering temperatures for cermet-based electrodes (>1000 °C). Hence, we first made the bi-layered electrolyte cells using a typical sintering process expecting the change of the electrolyte structure.

A single wavelength ellipsometer was used to measure the thickness of as-deposited YSZ layers by ALD (ALD-YSZ). The measured thicknesses with the number of ALD pulsing cycles is shown Fig. 1(b); the thicknesses of YSZ after 350, 700 and 1400 cycles were 28, 63 and 150 nm, respectively. For the sake of convenience, we labeled the four different kinds of bi-layers pure GDC (no YSZ layer), 28YG, 63YG and 150YG, where the numbers represent the YSZ thickness in nanometers. Insets of Fig. 1(b) are cross-sectional FE-SEM images for the 63YG and 150YG. These images show agreement with the ellipsometry measurements. An XPS analysis was also performed on the YSZ surfaces of as-deposited bi-layered electrolytes. Shown in Fig. 1(a), the XPS profiles obtained on the surfaces of the 28YG and 63YG films show only Y and Zr peaks without any Gd or Ce peaks [24]. The absence of Gd or Ce peaks indicates that the underlying GDC is entirely covered by the thin ALD-YSZ layers.

After screen-printing the GDC–NiO anode and GDC–LSCF cathode on each of the four bi-layered electrolytes, we measured the OCVs of the resulting cells. Note that the electrode screen-printing process required high temperature sintering steps (1400 °C for anodes and 1200 °C for cathodes). A simplified schematic drawing of the electrochemical measurement setup is presented in Fig. 2(a). The OCV with the humidified 5% H_2 fuel for the 63 YG and pure GDC cells shown in Fig. 2(b) decreased gradually over time and eventually dropped below 0.8 V after ~8 h. Nevertheless, the cell with the thickest YSZ protection layer (150YG cell) maintained an OCV of ~0.94 V throughout the measurement. This value is very close to the Nernstian voltage (0.95 V) under the given temperature and gas environment. The functionality of the bi-layer was further studied by varying the H_2 concentration. By increasing H_2 concentration, the thermodynamically determined Nernstian potential will *increase* by an amount proportional to the logarithm of H_2 concentration. On the other hand, a higher H_2 concentration will facilitate the chemical reduction of the ceria electrolyte, causing higher electronic leakage and thus a *decrease* in OCV. These two contributions are also reflected in the OCV profile of the 150YG (red line in Fig. 2(c)); Up to 20% H_2 concentration, the influence of thermodynamics is apparent. At higher concentrations, however, the degradation of electrolyte became predominant due to the ceria reduction. From these OCV measurements, it was verified that the bi-layered electrolyte exposed to sintering temperature is vulnerable to a highly reducing environment even with a 150 nm thick YSZ. As a comparison, the same OCV measurement was performed on a cell with a zirconia-based electrolyte, which is widely known to be chemically stable under a wide range of temperatures and oxygen partial pressure ($p(O_2)$). We used a commercial 150 μm thick scandia stabilized zirconia based button cell (ScSZ; NEXTCELL-2.5, NexTech Materials Ltd., USA). The corresponding OCV profile shown in the green line in Fig. 2(c) actually displayed the predominant contribution from the Nernstian behavior (as opposed to the electrolyte degradation). From the comparison with the ScSZ-based cell, the OCV dependency of bi-layered cells on the H_2 concentration strongly suggests that it is especially due to the chemical reduction of the GDC layer resulting in an electronic short circuit.

As shown above, pure GDC and 63YG cells could not maintain decent OCV values, whereas the 150YG showed a value close to the theoretical data for the entirety of the experiment. The cross-sectional SEM images shown in Fig. 3 provide a partial explanation of this occurrence. The 150 nm thick YSZ layer, which is clearly visible in the as-deposited sample (Fig. 3(a)), became significantly obscure after being exposed to 1400 °C (Fig. 3(b)). (The bright area visible on top of the YSZ layer is a Pt film in order to minimize electronic charging during the SEM imaging.) The contrast between the two images may be an indication of a significant inter-diffusion between YSZ and GDC layers, which occurred during the high temperature sintering process [19]. Even though the YSZ layer is not clearly defined in Fig. 3(b), there is a thin dark region right below the Pt layer and a following gradient in brightness along the thickness direction. The stable OCV value of the 150YG cell shown in Fig. 2(b) can be explained by the remaining, non-mixed region (i.e., the thin dark region in Fig. 3(b)). It may have remained as a close-to-stoichiometric YSZ, and thus, still functioned as the protection layer although a significant portion of its thickness mixed with the neighboring GDC layer. In the same vein, the low OCV of the 63YG cell is ascribed to a complete inter-diffusion affecting the whole YSZ thickness. Since a significant increase in electronic conductivity is expected when YSZ is mixed with GDC [20], the amount of non-mixed YSZ can be a determining factor for the bi-layer functionality. Surprisingly, the OCV of the 63YG cell is even lower than that of the pure GDC cell. Though a more extensive study is needed to confirm the prediction, it may be attributed to the consumption of pure GDC film in the 63YG bi-layer by the inter-mixing process. This process will make the effective electronically insulating layer thinner, and result in a higher electronic leakage through the electrolyte.

We also studied how the structure and chemical composition of a YSZ/GDC film changes under various temperatures ranging from 600 °C to 1500 °C. (Note that a bi-layered cell with a GDC–NiO cermet-based anode is usually prepared at ~1500 °C.) In order to

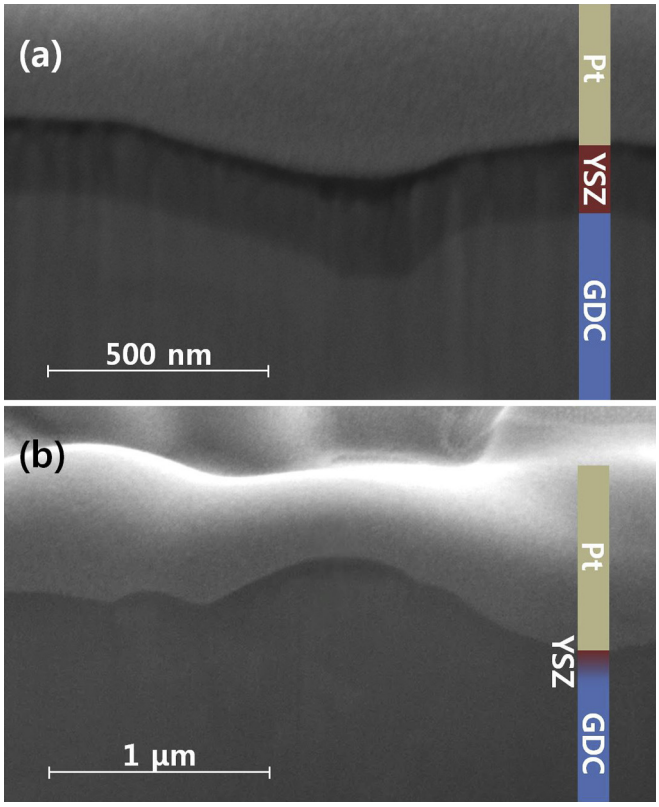

Fig. 3. A visual comparison between non-mixed and mixed bi-layered electrolytes (150YG sample). (a) The FIB-SEM image of as-deposited electrolyte shows the clear interface between GDC and YSZ. (b) The bi-layered sample exposed to a typical electrode sintering process lost significant contrast around the YSZ layer.

confirm the inter-diffusion between the YSZ and GDC, a set of depth-profiling XPS analyses was performed. Fig. 4 shows the XPS chemical profile along the depth direction of the 63YG sample which consisted of the 63 nm ALD-YSZ film and nano-polished GDC substrate. The as-deposited sample shows a sharp compositional transition around the YSZ/GDC interface as expected. The bi-layered sample exposed to 800 °C also does not show any Ce or Gd concentration around the film surface (the left-most part of the graphs). Nonetheless, the sample exposed to 1200 °C displayed a significant diffusion of its GDC into the YSZ layer; Ce concentration became especially significant around the surface of the bi-layered film. Exposure to 1500 °C made the whole film virtually uniform in chemical composition, indicating a complete mixture of the two layers. These results concur with a previous report by Zhou et al. showing changes in lattice parameter starting >1000 °C in a YSZ and GDC mixture [20].

Morphological thermal stability of the bi-layered electrolyte was also examined because even slight morphological variation can be highly detrimental to the functionality of an ultra-thin protection layer. Fig. 5 illustrates the surface topography images of a pure GDC and two YSZ/GDC bi-layer samples obtained after exposing the samples at different temperatures. The surface roughness of as-deposited film was below 2 nm regardless of the thickness of the YSZ protection layer. Furthermore, there was no significant roughness difference among the samples exposed to a temperature ≤800 °C. Combined with the XPS result in Fig. 4(b), it can be concluded that a fabrication temperature of ≤800 °C does not cause morphological or chemical complication to the nano-thin bi-layered electrolyte. However, samples exposed to 1200 °C start to show a significant change in the surface morphology. The GDC grain boundary of pure GDC became apparent while the grain size was virtually unchanged. One notable phenomenon observed in Fig. 5(k) is that the formation of YSZ grains is concentrated along the GDC grain boundaries. This is tentatively attributed to the natural preference of minimizing the overall surface energy. In a fuel cell operating environment, agglomerated YSZ along the GDC grain boundaries causes exposure of a significant portion of the GDC surface directly to the fuel. In this case, the YSZ layer would hardly function as a protection layer, and the chemical degradation rate should not be significantly different from a pure GDC. The 150YG sample in Fig. 5(l) also shows grain formation, but due to the thicker YSZ layer, the 'localized' agglomeration effect (i.e., agglomeration of YSZ along the grain boundaries of GDC) found on the 63YG sample was barely observed. Even so, the agglomeration may create unwanted physical paths of gas access to the GDC substrate. As shown in Fig. 5(m)–(o), the exposure to 1500 °C resulted in a dramatic increase in the grain size and surface roughness. Note that, the *z*-scales for these (m)–(o) samples are 10 times larger than the other images. The resulting grain size, which was even larger than the YSZ thicknesses, implies that the whole YSZ layer is likely to have been mixed with the underlying GDC. This was already proved by the XPS analysis in Fig. 4(d) and our anticipation of lower OCV of the 63YG cell than pure GDC cell in Fig. 2(b) was supported by these results.

Up to this point, we have discussed the thermal stability of bi-layered electrolytes during a sintering process where the electrolyte is in an air-based environment. Fig. 6 shows the morphological evolution of a bare GDC and bi-layers under an operational environment (where wet H_2 and air are provided to anode and cathode, respectively). When the pure GDC was exposed to humidified H_2, the roughness increased by a factor of 3 (from 1.90 to 5.94 nm) at 600 °C. Note that no significant change in roughness was observed in air at the same temperature. The origin of roughness is micro-crack generation in ceria due to the internal stress between a reduced (expanded) surface and a non-reduced internal region

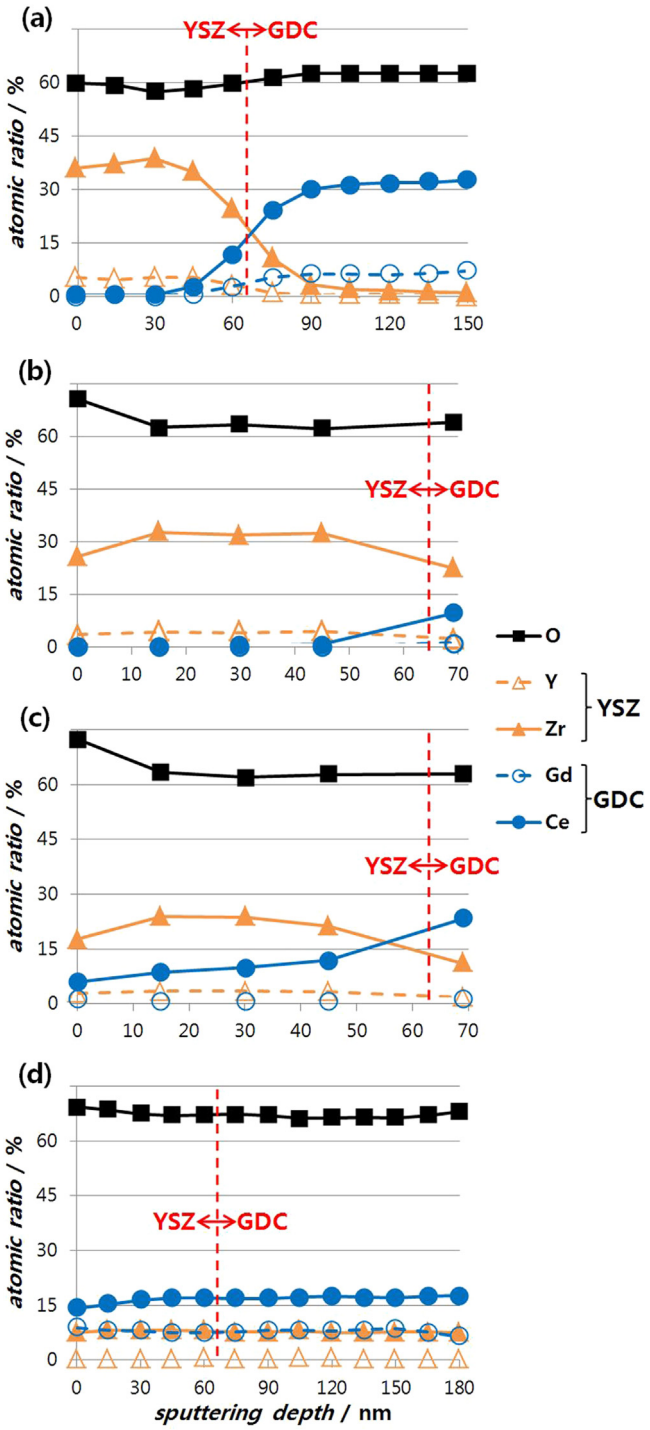

Fig. 4. XPS depth profiles of 63YG electrolytes exposed to various temperatures. Red dashed lines indicate the original interface between YSZ and GDC and "0 nm" sputtering depth means the sample surface. (a) As-deposited 63YG and 63YG samples exposed to (b) 800 °C, (c) 1200 °C, and (d) 1500 °C (For interpretation of the references to color in this figure legend, the reader is referred to the web version of this article.).

[25]. If the thickness of YSZ is not enough to protect GDC from reduction, the roughness evolution of the GDC surface affects the structure of YSZ layer and makes the layer permeable to fuel gas. At lower temperatures, the YSZ protection layer better serves its role under the reducing environment for an extended period of time (100 h). At 600 °C, the change in roughness was minimal, even with the thinnest YSZ layer (28 nm). At 800 °C, however, only the sample

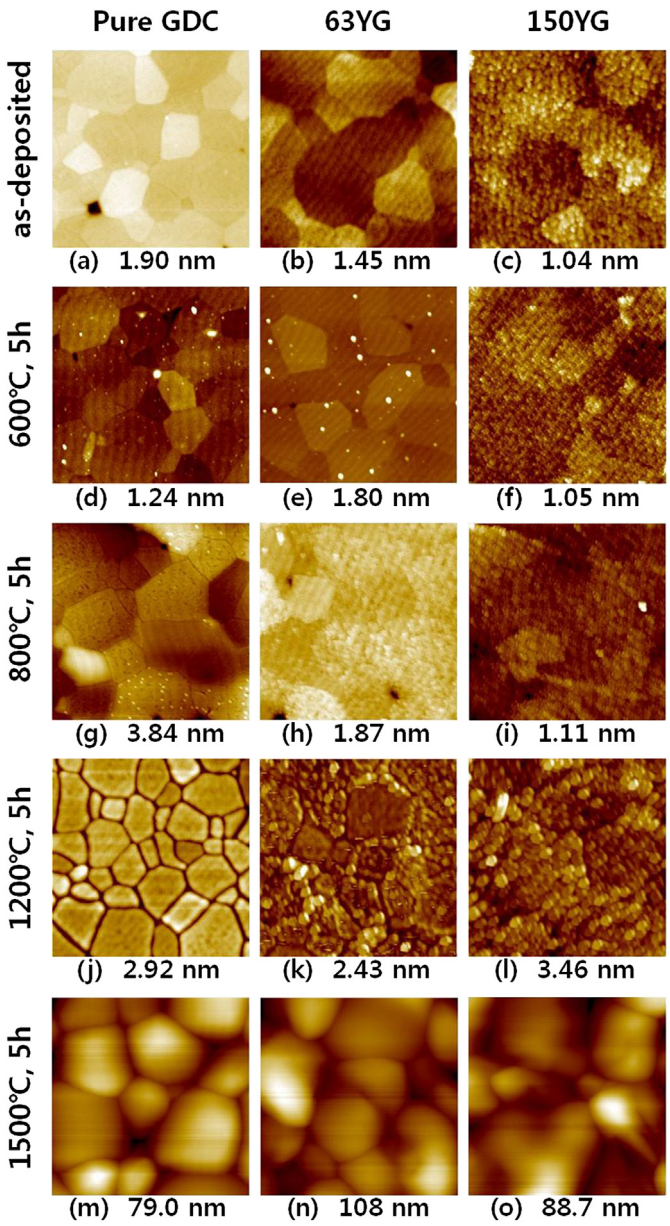

Fig. 5. AFM topography images of pure GDC, 63YG and 150YG samples obtained after exposing them to various temperatures. The scanned areas are $4 \times 4\ \mu m^2$ and the *z*-scales for (m), (n) and (o) are 10 times larger than the other images. The numbers are RMS values of roughness.

with the thickest (150 nm) YSZ layer showed roughness stability. With these results, we can determine that the critical operational condition necessary for the stability of a bi-layer exists for the given thickness of protective layer.

3.2. Cells without exposure to high temperatures

In the previous section, we observed that high temperature sintering ($>\sim$1000 °C) causes significant morphological and compositional changes and thus dismantles the function of the thin YSZ protection layer. In order to study the effect of the YSZ layer as a chemical stabilizer during an SOFC operation excluding the impact of these morphological/chemical changes, the fabrication and operational temperatures were limited up to only 600 °C. Fig. 7 shows the time evolution of OCV measured at 600 °C for a pure GDC sample and three bi-layered samples with different ALD-YSZ thicknesses (28, 63 and 150 nm thick). We used sputtered Pt as both anode and cathode because typical wet methods of ceramic electrodes necessitate high temperature sintering processes. Compared to humidified H_2, dry H_2 in these OCV measurements renders lower $p(O_2)$, and therefore is a harsher environment for ceria-based electrolytes. Even under the harsh environment, all the ALD-YSZ coated cells showed stable OCVs of $>$1 V even after $\sim$80 h, whereas the GDC cell without a YSZ protection layer displayed a significant decrease in OCV over time ($<$0.6 V after $\sim$50 h). It is noteworthy that even the 28 nm thick ALD-YSZ layer successfully acted as a protective layer enabling a long-term operation of the cell, even under dry H_2 environment. To the best of our knowledge, there has been no previous report showing such a long-term stability of ceria-based cells using a nano-thin protection layer.

After 80 h-long OCV measurements of the 28YG cell at 600 °C, the cell temperature was raised to 800 °C at 4 °C min^{-1}. At first we

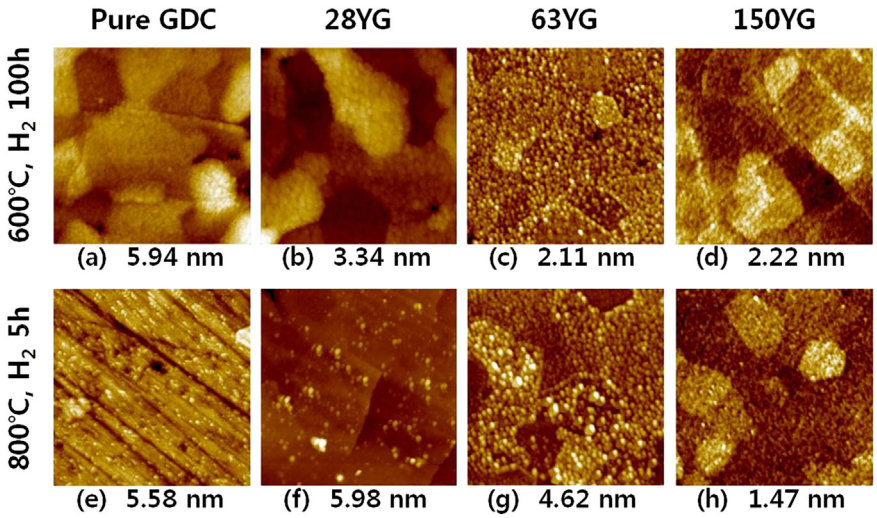

Fig. 6. AFM topography images of pure GDC, 63YG and 150YG samples obtained after exposing them to 600 °C and 800 °C under humidified H_2 environments. The scanned areas are 4 × 4 μm^2. The numbers are RMS values of roughness.

observed a fast OCV drop (4.4 mV min^{-1}) at 800 °C, then we decreased the temperature at the rate of −4 °C min^{-1}. When the temperature reached back to 600 °C, the OCV was 0.97 V, but dropped to 0.89 V in 10 min. The OCV loss was not recovered even after hours of operation at 600 °C; the damage to the cell was permanent once incurred.

3.3. Advantage of ALD as the protection layer deposition technique

Although PVD techniques such as AC magnetron sputter deposition and pulsed laser deposition (PLD) have been widely used to deposit functional layers at relatively low temperatures [11–14,26,27]. We considered the ALD technique more advantageous in depositing a pinhole-free and highly uniform protection layer. The postulated advantages become evident when the current work is compared to a recent work performed by Myoung et al. in which the PLD technique was used to deposit the protection layer [14]. They reported a similar YSZ/GDC bi-layer study. The thickness of YSZ varied between 25 and 200 nm while that of GDC was 1 μm. As expected, the OCVs from the cells scattered less as the YSZ thickness increased. However, the OCVs were close to the theoretical value (>1 V) even with a YSZ thickness as thin as 25 nm. Though their report successfully presented the role of a nano-thin protection layer, it is still worthwhile to compare their result with those presented in this report as detailed below.

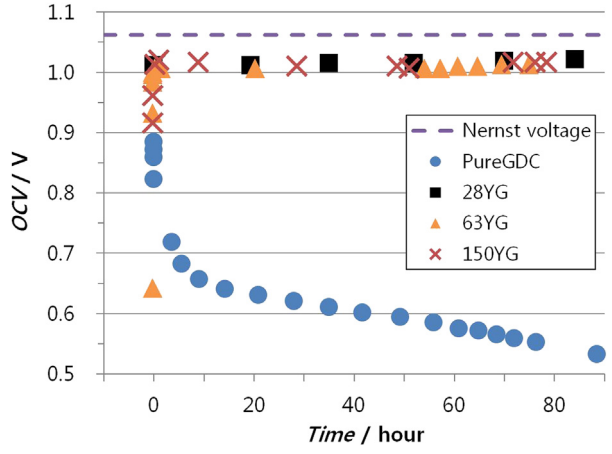

Fig. 7. Time evolution of OCV under dry H_2 at 600 °C for the pure GDC (blue circle), 28YG (black rectangle), 63YG (yellow triangle) and 150YG (red cross) cells. These cells were not exposed to a temperature above 600 °C. All the ALD based bi-layered cells including 28YG (with a YSZ-GDC thickness ratio of 6.5 × 10^{-5}) maintained OCVs over 1 V for ~80 h (For interpretation of the references to color in this figure legend, the reader is referred to the web version of this article.).

Recently, Kwon et al. analytically predicted the minimum thickness of the YSZ layer required to protect the neighboring GDC layer from reduction [28]. The electronic and ionic conductivities of both GDC and YSZ were obtained from the given oxygen activity and temperature, which was in accordance with previous reports [2,3,29]. Based upon the known ionic/electronic conductivities and charge conservation criterion, they deduced expressions to predict the YSZ/GDC thickness ratio that would have both the electrolytes stay in the "electrolytic domain". The electrolytic domain is defined as the situation where the ionic transfer number is larger than 0.5. The resulting equations to quantify $p(O_2)$ on the fuel side and the thickness ratio required to be in the electrolytic domain read as follows [28,30].

$$P_{O_2} = \left(\frac{P_{H_2O}}{P_{H_2}}\right)^2 \cdot e^{\frac{\Delta G}{RT}} \tag{1}$$

$$\frac{t_{YSZ}}{t_{YSZ}+t_{GDC}} = 1 - \left[1 + \frac{\sigma_{ion}^{YSZ} \ln \frac{P_{O_2}^{n,YSZ-1/4} + P_{O_2}^{'''-1/4}}{P_{O_2}^{n,YSZ-1/4} + P_{O_2}^{''-1/4}}}{\sigma_{ion}^{GDC} \ln \frac{P_{O_2}^{n,GDC-1/4} + P_{O_2}^{''-1/4}}{P_{O_2}^{n,GDC-1/4} + P_{O_2}^{'-1/4}}}\right] \tag{2}$$

where ΔG is standard free energy change for H_2/H_2O reaction and σ_{ion} is ionic conductivity. P'_{O_2}, P''_{O_2} and P'''_{O_2} denote the $p(O_2)$ at the air, YSZ/GDC interface and fuel side, respectively. At least, $P^n_{O_2}$ must be at the lower electrolytic boundary (or reducing boundary) where the electronic and ionic conductivities are the same, i.e., this is a material property.

In Myoung et al.'s work mentioned above, 3% humidified H_2, equivalent to the $p(O_2)$ of 1.58 × 10^{-22} Pa, was used as the fuel. In this case, the minimum YSZ thickness required to be in the electrolytic domain is 1.4 × 10^{-7} of the GDC thickness. However, their bi-layer, even with a much higher thickness ratio (25 nm thick YSZ; equivalent to the thickness ratio of 2.5 × 10^{-2}), could not render a stable OCV; it resulted in a significant OCV scattering from 0.45 to 1.05 V. Our fuel, on the other hand, was dry H_2 (99.999%), equivalent to a

$p(O_2)$ of $1.65 \times 10^{-29} - 1.65 \times 10^{-31}$ Pa. The finite range in the $p(O_2)$ came from the specified variations in the H_2O content among its impurities. The corresponding minimum YSZ thickness needed to suppress electronic conduction was $9.7 \times 10^{-6} - 3.1 \times 10^{-5}$ of GDC thickness. The required thickness was thicker than what was needed in the humidified H_2 by almost two orders. Despite the disadvantage, our ALD-based YSZ/GDC cell showed a very stable and high OCV, even with a thickness ratio of 6.5×10^{-5}. This ratio is very close to the theoretically required value (see Table 1). The YSZ layer was only 2.1–6.7 times thicker than the calculated thickness.

The discrepancy in the functionality of these two different kinds of blocking layers (one deposited by ALD and the other by PLD) is mainly accredited to the difference in their microstructures. Reportedly, there are inevitable voids and pinholes in YSZ layers deposited on a porous (rough) substrate by PLD [31]. Selective nucleation, columnar growth on a rough substrate and grain growth in the lateral direction were considered to cause voids and pinholes in the PLD-YSZ film, especially in the regions closer to the substrate. These voids and pinholes were also believed to be the source of the gas leakage and lowered OCV. Considering Myoung et al. used the PLD technique to deposit the 25 nm YSZ layer, the unstable OCV can be attributed to the voids and pinholes in the film. The non-conformal step coverage of the PLD-YSZ film might have resulted in a direct access of fuel (humidified H_2) to the ceria surface and caused the OCV to become unstable. Another reason for the unstable OCV can be found in the lack of thickness uniformity, which is often observed in films created by PVD techniques. The PVD film thickness has a strong dependency on the distance and angle from the target [32]. Consequently, the resulting YSZ thickness varies even in the same sample and the functionality of ceria protection can fall below the expected critical point in some areas. The ALD-based film, however, suffers significantly less from these uniformity and void formation issues. In one study, Shim et al. compared the morphologies and the performances of anhydrous proton conducting yttria-doped barium zirconia electrolytes prepared by ALD and PLD [33]. They ascribed the difference in the performance to the surface morphology differences. In the AFM analysis, they observed that the ALD films showed close-packed circular grains with surface roughness of <1 nm while the PLD films consisted of loosely packed grains with a larger roughness of 2 nm.

To confirm the protection effect of ALD-YSZ on a rough GDC surface, SEM images were taken from the anode-side surfaces of pure GDC and ALD-based 28YG electrolytes. We obtained the images before and after exposing them to a cell operational condition (600 °C in a highly reducing dry 99.999% H_2) for ~80 h. Numerous nano-cracks were found to appear on the surface of pure GDC after the operation as shown in Fig. 8(b), but no significant surface damage was observed on the ALD-YSZ surface (Fig. 8(d)). This visual comparison reassures the functionality of an ALD-based nano-thin YSZ protection layer under a reducing environment.

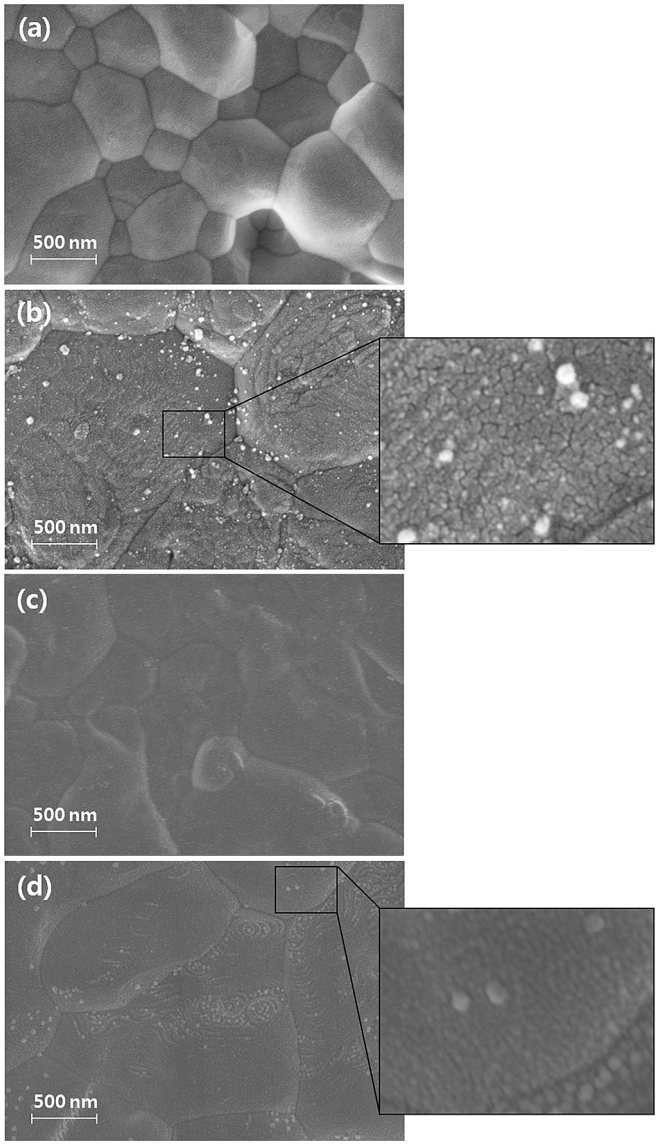

Fig. 8. SEM images of pure GDC and 28YG cells on the anode side obtained before and after exposure to an operational condition (dry H_2 at 600 °C) for ~80 h; pure GDC (a) before and (b) after operation for ~80 h. 28YG (c) before and (d) after operation for ~80 h. While numerous nano-cracks were found on the surface of pure GDC after the operation, no significant surface damage was observed on the 28YG sample (with an extremely low YSZ/GDC thickness ratio of 6.5×10^{-5}).

4. Conclusions

In order to maximize ionic conduction, oxygen reduction reaction and chemical stability of IT-SOFC simultaneously, YSZ/GDC bi-layered electrolyte has been often explored. The YSZ film in a bi-layer is expected to function as a protective layer preventing the underlying GDC film from being chemically reduced on the anode side. It is desirable to have the YSZ layer as thin as possible because of its relatively low ionic conductivity in the intermediate temperature range (600–800 °C) compared to GDC. In this study, first, the degree of chemical inter-diffusion across the ALD-YSZ/GDC

Table 1
Comparison of theoretically determined YSZ/GDC thickness ratios (r) with those of experimental ratios for both ALD and PLD-based bi-layers.

	ALD-YSZ/GDC cell with dry H_2			PLD-YSZ/GDC cell with humidified H_2 [14]			
t_{actual} (YSZ)	28 nm	63 nm	150 nm	25 nm	50 nm	100 nm	200 nm
r_{actual} (YSZ/GDC)	6.5×10^{-5}	1.5×10^{-4}	3.5×10^{-4}	2.5×10^{-2}	5.0×10^{-2}	0.1	0.2
$r_{required}$ (YSZ/GDC)	$9.7 \times 10^{-6} - 3.1 \times 10^{-5}$			1.4×10^{-7}			
$t_{actual}/t_{required}$	2.1–6.7	4.8–15	11–36	1.8×10^{5}	3.6×10^{5}	7.3×10^{5}	1.5×10^{6}
OCV status	Stable	Stable	Stable	Unstable	Stable	Stable	Stable

boundary was evaluated with respect to sample fabrication temperature using cross-sectional SEM imaging and XPS analysis. A significant penetration of GDC, especially Ce species, into the YSZ layer was observed in the bi-layered electrolyte with the temperature of 1200 °C and higher. In addition, AFM topography images displayed localized agglomeration of small YSZ grains along the grain boundaries of the underlying GDC film (at 1200 °C). Low OCV values from bi-layer electrolyte-based cells sintered at these high temperatures were well aligned with the observed phenomena. When the YSZ side faces dry H_2 fuel, OCV values of the cell not exposed to high temperature remained close to the Nernstian potential even after 80 h of operation, even with 28 nm thick ALD-YSZ, as long as the temperature is $\leq$600 °C. This study also discussed the functionality of ALD-YSZ protection layers compared to that of YSZ layers deposited by the PLD method. Based on this study, many other SOFC structures with thinner electrolyte (e.g. anode/cathode supported type, self-supporting thin film type) might also adopt the ALD technique to form a functional layer and can avoid the loss of stability and performance with the fabrication/operation guidelines we suggested here.

Acknowledgments

This work was supported by the Global Frontier R&D Program on Center for Multiscale Energy System funded by the National Research Foundation under the Ministry of Science, ICT & Future, Korea (No. 2011-0031567) and also supported by a Start-up Research Grant of the University of California, Merced. The authors would like to thank Seungbum Ha (Nanyang Technological University), Joon Hyoung Shim (Korea University) and Jinha Hwang (Hongik University) for their help with sample preparation, Seyun Lah (Samsung SDI, Korea) and Hoon Choi (Seoul National University) for the experimental setup, and Taehyun Park, Jongwoo Choi and Sanghoon Ji (Seoul National University) for their advice in characterization processes.

References

[1] R.P. O'Hayre, S.W. Cha, W. Colella, F.B. Prinz, Fuel Cell Fundamentals, second ed., John Wiley & Sons, Hoboken, USA, 2009. Ch. 8.
[2] J.H. Park, R.N. Blumenthal, J. Electrochem. Soc. 136 (1989) 2867–2876.
[3] B.C.H. Steele, Solid State Ionics 129 (2000) 95–110.
[4] V.V. Kharton, F.M.B. Marques, A. Atkinson, Solid State Ionics 174 (2004) 135–149.
[5] S.C. Singhal, K. Kendall, High Temperature Solid Oxide Fuel Cells: Fundamentals, Design and Applications, first ed., Elsevier Advanced Technology, Oxford, UK, 2003. Ch. 4.
[6] A. Atkinson, Solid State Ionics 95 (1997) 249–258.
[7] I. Yasuda, K. Hishinuma, in: Proceedings of the Third International Symposium on Ionic and Mixed Conducting Ceramics, 1998, pp. 178–186.
[8] H. Yahiro, Y. Baba, K. Eguchi, H. Arai, J. Electrochem. Soc. 135 (1988) 2077–2080.
[9] E.D. Wachsman, P. Jayaweera, N. Jiang, D.M. Lowe, B.G. Pound, J. Electrochem. Soc. 144 (1997) 233–236.
[10] X.G. Zhang, M. Robertson, C. Deces-Petit, Y.S. Xie, R. Hui, S. Yick, E. Styles, J. Roller, O. Kesler, R. Maric, D. Ghosh, J. Power Sources 161 (2006) 301–307.
[11] J.Y. Park, E.D. Wachsman, Ionics 12 (2006) 15–20.
[12] D.F. Yang, X.G. Zhang, S. Nikumb, C. Deces-Petit, R. Hui, R. Maric, D. Ghosh, J. Power Sources 164 (2007) 182–188.
[13] K. Mehta, S.J. Hong, J.F. Jue, A.V. Virkar, in: Proceedings of the Third International Symposium on Solid Oxide Fuel Cells, 1993, pp. 92–103.
[14] D.H. Myung, J. Hong, K. Yoon, B.K. Kim, H.W. Lee, J.H. Lee, J.W. Son, J. Power Sources 206 (2012) 91–96.
[15] P. Soral, U. Pal, W.L. Worrell, J. Electrochem. Soc. 145 (1998) 99–106.
[16] H.T. Lim, A.V. Virkar, J. Power Sources 192 (2009) 267–278.
[17] X.E. Zhang, J. Gazzarri, M. Robertson, C. Deces-Petit, O. Kesler, J. Power Sources 185 (2008) 1049–1055.
[18] Q.L. Liu, K.A. Khor, S.H. Chan, X.J. Chen, J. Power Sources 162 (2006) 1036–1042.
[19] A. Tsoga, A. Gupta, A. Naoumidis, P. Nikolopoulos, Acta Mater. 48 (2000) 4709–4714.
[20] X.D. Zhou, B. Scarfino, H.U. Anderson, Solid State Ionics 175 (2004) 19–22.
[21] R.D. Shannon, C.T. Prewitt, Acta Crystallogr. Sec. B. B25 (1969) 925–946.
[22] L. Niinisto, M. Ritala, M. Leskela, Mater. Sci. Eng. B-Solid. 41 (1996) 23–29.
[23] J.H. Shim, C.C. Chao, H. Huang, F.B. Prinz, Chem. Mater. 19 (2007) 3850–3854.
[24] J.F. Moulder, W.F. Stickle, P.E. Sobol, K.D. Bomben, Handbook of X-ray Photoelectron Spectroscopy: A Reference Book of Standard Spectra for Identification and Interpretation of XPS Data, Physical Electronics, Chanhassen, USA, 1995.
[25] M. Mogensen, T. Lindegaard, U.R. Hansen, G. Mogensen, J. Electrochem. Soc. 141 (1994) 2122–2128.
[26] T.P. Tsai, E. Perry, S. Barnett, J. Electrochem. Soc. 144 (1997) L130–L132.
[27] S.Q. Hui, D.F. Yang, Z.W. Wang, S. Yick, C. Deces-Petit, W. Qu, A. Tuck, R. Maric, D. Ghosh, J. Power Sources 167 (2007) 336–339.
[28] T.H. Kwon, T. Lee, H.I. Yoo, Solid State Ionics 195 (2011) 25–35.
[29] NexTech Materials Ltd. http://www.fuelcellmaterials.com/site/images/stories/PDFs/cerias.pdf, 2008.
[30] R.T. DeHoff, Thermodynamics in Materials Science, second ed., CRC Press, Boca Raton, USA, 2006. Ch. 11.
[31] C.W. Kwon, J.W. Son, J.H. Lee, H.M. Kim, H.W. Lee, K.B. Kim, Adv. Funct. Mater. 21 (2011) 1154–1159.
[32] F.E. Fernandez, J. Vac. Sci. Technol., A. 13 (1995) 421–427.
[33] J.H. Shim, J.S. Park, J. An, T.M. Gur, S. Kang, F.B. Prinz, Chem. Mater. 21 (2009) 3290–3296.